Contents lists available at SciOpen

Food Science and Human Wellness

journal homepage: https://www.sciopen.com/journal/2097-0765

China Food Publishing Co.

Ginsenoside CK inhibits melanoma growth by promoting apoptosis and targeting cGAS-STING pathway to regulate the immune microenvironment

Haodong Tang[a,b,c], Ying Xu[a,b,c], Rongzhan Fu[a,b,c], Zhiguang Duan[a,b,c], Chenhui Zhu[a,b,c,*], Daidi Fan[a,b,c,*]

[a] *Shaanxi Key Laboratory of Degradable Biomedical Materials, School of Chemical Engineering, Northwest University, Xi'an 710069, China*
[b] *Shaanxi R&D Center of Biomaterials and Fermentation Engineering, School of Chemical Engineering, Northwest University, Xi'an 710069, China*
[c] *Biotech & Biomed Research Institute, Northwest University, Xi'an 710069, China*

ARTICLE INFO

Article history:
Received 13 May 2024
Received in revised form 14 June 2024
Accepted 16 December 2024

Keywords:
Ginsenoside compound K
STING
Apoptosis
Melanoma
$CD8^+$ T cell
Tumor immune microenvironment

ABSTRACT

Malignant melanoma, the 19th most prevalent cancer globally, is the primary cause of mortality attributed to cutaneous malignancies. Ginsenoside compound K (CK), a rare ginsenoside renowned for its potent medicinal properties and established safety profile, is widely employed in the treatment and prevention of various diseases. This study aimed to investigate the influence of CK on cyclic GMP-AMP synthase-stimulator of interferon genes (cGAS-STING) pathway in melanoma, particularly its effects on apoptosis and the immune microenvironment, with the ultimate goal of impeding melanoma growth. In the present study, we used a subcutaneous hormonal tumor model in homozygous mice to investigate whether CK has an inhibitory effect on melanoma growth. The effect of CK on melanoma cell apoptosis was analyzed by flow cytometry, immunohistochemistry, hematoxylin and eosin staining, protein immunoblotting, and RT-qPCR were used to observe the effect of CK on melanoma cytokines. The effects of CK on cGAS-STING pathway in melanoma cells were investigated by protein immunoblotting, immunofluorescence, flow cytometry and molecular docking. The findings demonstrate that CK effectively suppresses melanoma cell proliferation. Molecular docking analysis revealed a binding energy of –6.59 kcal/mol between CK and STING, indicating the potential of CK as a targeted regulator of STING. Mechanistically, CK induces apoptosis in melanoma cells through the Caspase pathway and enhances STING-mediated regulation of the immune microenvironment *via* the cGAS-STING pathway, thereby inhibiting melanoma growth. Notably, our study provides the first evidence that CK acts as an immune checkpoint agonist, elevating T lymphocyte levels within tumors. CK promotes apoptosis through the Caspase pathway, regulates the cGAS-STING pathway, promotes the production of IFN-β and chemokines by the nucleus, and promotes the infiltration of T-cells in the tumor microenvironment, thus achieving the inhibition of melanoma.

1. Introduction

Malignant melanoma is a rare neoplasm caused by melanocytes, which are cells responsible for producing melanin. According to the data from the World Health Organization, in the year 2020, there were 3.4 cases of malignant melanoma per 100 000 individuals worldwide[1]. However, malignant melanoma is also the most lethal type of skin cancer, accounting for 65% of skin cancer-related deaths, despite representing only 4% of skin cancer cases[2].

In recent decades, various chemical drugs have been employed for the treatment of melanoma. Chemotherapy, as a systemic adjuvant therapy for melanoma, is associated with significant side effects, including anorexia, nausea, vomiting, and hepatic and renal impairments, and it only extends survival by a few months[3]. Therefore, the development of therapeutics that are both effective in treating malignant melanoma and reducing side effects is crucial for improving the quality of life for patients with this condition.

* Corresponding authors at: Shaanxi Key Laboratory of Degradable Biomedical Materials, School of Chemical Engineering, Northwest University, Xi'an 710069, China.
E-mail address: zch2005@nwu.edu.cn (C.H. Zhu); fandaidi@nwu.edu.cn (D.D. Fan)

Peer review under responsibility of Beijing Academy of Food Sciences.

SciOpen Publishing services by Tsinghua University Press

http://doi.org/10.26599/FSHW.2025.9250480

Stimulator of interferon genes (STING) is a transmembrane protein that functions as a crucial adaptor in the cytosolic DNA sensing pathway[4]. Upon binding of cytoplasmic DNA, cyclic GMP-AMP synthase (cGAS) triggers the production of cyclic GMP-AMP (cGAMP), which binds to and activates STING, leading to the generation of immune mediators and inflammatory cytokines[5]. Increasing evidence suggests that the cGAS-STING pathway plays a significant role in tumor formation and cancer immune surveillance[6]. The major mechanism of tumor intrinsic immune sensing occurs through STING-dependent cytoplasmic DNA sensing within tumor-infiltrating dendritic cells (DCs). Additionally, studies have demonstrated that the production of mitochondrial reactive oxygen species (ROS) can result in the formation of oxidized mitochondrial DNA. Oxidized cytoplasmic DNA can enhance STING-dependent type I interferon (IFN-I) induction and activate the STING signaling pathway[7]. Activation of STING can promote the efficacy of radiotherapy, induce autophagy in HeLa cells and mouse fibroblasts, and activate innate immune responses[8-9]. STING agonists can induce apoptosis in malignant B cells[10]. Moreover, *in vivo* studies have shown that STING activation exhibits potent anti-tumor effects by inducing local innate responses and systemic adaptive immune responses[11]. However, the inhibition of the cGAS-STING pathway has been observed in most tumors. In samples of malignant melanoma, the expression of STING is associated with tumor stage, with significant inhibition of STING observed in advanced-stage tumors. Recent research has indicated that STING protein expression is undetectable or significantly suppressed in 6 malignant melanoma cell lines, and downregulation of the cGAS-STING signaling pathway can induce tumor cell resistance to immune effector molecules[12]. Therefore, the search for STING agonists is of paramount importance in immunotherapy for melanoma.

Ginseng, a precious traditional Chinese medicinal herb, possesses multiple biological effects[13]. Its main active component is ginsenoside, which exhibits anti-tumor[14], anti-inflammatory[15], anti-aging[16], anti-diabetic[17], neuroprotective[18], and immune-enhancing properties[19]. Ginsenoside compound K (CK) (Fig. 1A), a rare ginsenoside, also exhibits inhibitory effects on the development of various cancers. For instance, CK inhibits the expression of the anti-apoptotic protein Bcl-2 and the apoptosis-related pathway PI3K/AKT/NF-κB, thereby suppressing the proliferation and activity of HGC-27 gastric cancer cells *in vitro* and *in vivo*[20]. CK can inhibit the proliferation of triple-negative breast cancer by suppressing glutamine metabolism and promoting cell apoptosis[21]. Moreover, CK can inhibit hypoxia-induced epithelial-mesenchymal transition in liver cells by inhibiting the HIF-1α/NF-κB signaling pathway[22]. However, the research on the impact of CK on the immune system is limited. Furthermore, the role and potential mechanisms of CK in melanoma remain largely unexplored.

In this study, we investigated the anti-tumor effects of CK on the cGAS-STING pathway target in melanoma and explored the potential molecular mechanisms underlying these effects both *in vitro* and *in vivo*. We discovered that CK acts to promote STING phosphorylation, activating its activity and increasing the phosphorylation of TANK-binding kinase 1 (TBK1) as well as the expression of IFN-I. Additionally, CK increased the proportion of T lymphocytes in tumor tissues, effectively promoting the anti-tumor immune activity in melanoma mice. The findings of this study provide solid scientific evidence for the application of CK in immunotherapy for melanoma.

2. Materials and methods

2.1 Reagents and antibody

Roswell Park Memorial Institute-1640 (RPMI-1640), fetal bovine serum (FBS), penicillin, and streptomycin were all sourced from Gibco (Grand Island, NY, USA). CK was provided by the Institute of Biomedical and pharmaceutical sciences, Northwest University (Xi'an, China). The STING inhibitor C 170 was procured from MedChemExpress (New Jersey, USA). The bicinchoninic acid (BCA) protein assay kit was obtained from Solarbio (Beijing, China). A saline solution was provided by Huarun Shuanghe (Beijing, China). Ethanol was acquired from Zhongjinlong Technology (Chengdu, China). The antibodies utilized in this study are presented in Table S1.

2.2 Cell culture

The B16F10 melanoma cells (Mus musculus, mouse) utilized in this study were obtained from the Chinese Academy of Sciences Committee on Type Culture Collection Cell Bank (Shanghai, China). These cells were cultured in RPMI-1640 medium supplemented with 10% FBS, 100 U/mL penicillin, and 100 g/mL streptomycin. Cultivation was carried out in a controlled environment at 37 °C with 5% CO_2. Subculturing was performed at passage ratios ranging from 1:2 to 1:10. It is pertinent to note that in this research, B16F10 cells exhibited negative results for mycoplasma contamination, and their doubling time was approximately 24 h.

2.3 Cell viability assay

To evaluate the impact of CK on cell proliferation, cells were seeded in a 96-well plate at a density of 1×10^4 cells/well, with each well containing 100 μL of culture medium. For cytotoxicity assessment, after 24 h of incubation, fresh medium supplemented with varying concentrations of CK was added to the wells, followed by an additional 24- and 48-h incubation. In all experiments, 50 μL of 3-(4,5-dimethylthiazol-2-yl)-2,5-diphenyltetrazolium bromide (MTT) solution (5 mg/mL, obtained from Solarbio, Beijing, China) was added to each well, and the cells were incubated at 37 °C for 3 h. Subsequently, formazan crystals were dissolved by adding 150 μL of dimethyl sulfoxide (DMSO) (Aladdin Biotechnology, Shanghai, China), and the absorbance was measured at 490 nm.

2.4 Hoechst 33342 staining

After exposure to varying concentrations of CK, B16F10 cells were rinsed with PBS and subsequently co-incubated with Hoechst 33342 (sourced from Solarbio, Beijing, China) following a 24-h incubation period. After a 20-min staining duration, morphological alterations were observed using a fluorescence microscope (Nikon, Japan).

2.5 Acridine orange/ethidium bromide (AO/EB) staining

A cell population of 1×10^5 cells/mL was cultured in 2 mL of medium in a 6-well plate for 24 h. Subsequently, cells were subjected to treatment with different concentrations of CK and stained using AO/EB (Yuanye, Shanghai, China). Photomicrographs were captured using a fluorescence microscope (Nikon, Japan).

2.6 Animal experiments

All animal experiments were conducted with approval from the Northwest University Animal Welfare Committee (NWU-AWC-20210313M). C57BL/6 mice (4–6 weeks old, 12–16 g) were procured from GemPharmatech Co., Ltd. (Nanjing, China). One million B16F10 cells suspended in 100 μL serum-free RPMI-1640 were injected into the left axilla of each mouse. Once tumor volumes reached 80–100 mm^3, mice were divided into different groups (n = 8): Normal group, Normal + CK group (80 mg/(kg·day)), Control group (intraperitoneal injection of solvent), L-CK group (40 mg/(kg·day)), H-CK group (80 mg/(kg·day)), and Cyclophosphamide group (10 mg/(kg·2 days)). The Control group received an intraperitoneal injection of solvent (a mixture of 87% saline, 8% polyethylene glycol castor oil, and 5% ethanol). CK and cyclophosphamide were weighed and dissolved in the solvent. Finally, the animals were euthanized, and tumors and organs were collected and stored at –80 °C for further analysis. The animal experiment design is shown in Fig. S1. The formula for calculating tumor volume was:

$$\text{Tumor volume } (mm^3) = 0.5 \times \text{Length (mm)} \times \text{Width}^2\,(mm^2)$$

2.7 Extraction of tumor infiltrating lymphocytes

To isolate infiltrating lymphocytes from tumors, euthanasia was performed on the mice, followed by careful dissection of the tumor tissues. Using ophthalmic scissors, the tumor was minced into small fragments and subsequently immersed in whole blood and tissue dilution buffer. The mixture was centrifuged at 500 × g for 5 min to pellet the tumor tissues at the bottom. The tumor fragments were then resuspended in 10 mL of tissue digestion solution (RPMI-1640 cell culture medium supplemented with 10% FBS, 2 units/mL hyaluronidase (Yuanye Bio-Tec, Shanghai, China), 1 mg/mL type IV collagenase (Yuanye Bio-Tec, Shanghai, China), and 1 mg/mL DNase (Yuanye Bio-Tec, Shanghai, China) and incubated on a shaking platform for 45 min. Following digestion, the processed tumor tissue was passed through a 70 μm cell strainer to ensure proper filtration. Subsequently, infiltrating lymphocytes were isolated from the tumor tissue using a mouse tumor infiltrating lymphocyte separation kit (Solarbio, Beijing, China).

2.8 Flow cytometry analysis

To harvest CK-treated cells, cells were carefully washed and stained with DCFH-DA in a light-protected environment for 20 min. Subsequently, the mean fluorescence intensity (MFI) of the cells was quantified using a flow cytometer (BD Accuri C6 Plus, USA).

CK-treated cells were collected, and JC-1 staining working solution was added for light-protected staining for 20 min. Following this, the supernatant was centrifuged, and the cells were subjected to 2 washes with JC-1 staining buffer. The cells were then pelleted, resuspended in JC-1 staining buffer, and subjected to machine-based analysis.

After collecting the cells subsequent to CK treatment, the cell concentration was adjusted to 3×10^6 cells/mL using an appropriate buffer. A volume of 100 μL of the cell suspension was then aspirated, to which 5 μL of Annexin V/FITC was added. The mixture was thoroughly mixed and incubated in the absence of light for 5 min. Following this incubation period, 5 μL of propidium iodide (PI) solution and 400 μL of PBS were added. The assay was subsequently conducted using a flow cytometer.

A total of 100 μL of the isolated tumor-infiltrating lymphocyte suspension was aliquoted, and 5 μL of the CD16/32 blocking antibody was added. The mixture was allowed to incubate at room temperature for 10 min for appropriate blocking. Following this, 3 μL FITC-CD45, 1 μL each of PerCP-CD3, APC-CD4, and PE-CD8 antibodies were added, and the samples were incubated in the dark at 4 °C for 30 min. After incubation, the samples were centrifuged at 150 × g for 5 min to pellet the cells. The cell pellet was then resuspended in 500 μL of PBS prior to analysis. Cell collection was conducted using a BD Accuri C6 Plus flow cytometer, and the results were analyzed using Flow Jo software (Tree Star Inc., OR, USA).

2.9 RNA isolation and RT-PCR analysis

Tumor tissue RNA extraction was performed using TRIzol reagent (Invitrogen, Carlsbad, USA). Subsequently, cDNA was synthesized using the RevertAid First Strand cDNA Synthesis Kit and a reverse transcription system (Thermo Fisher Scientific, Fremont, USA). qRT-PCR was conducted in a thermal cycler (Bio-Rad, USA) using FS Universal SYBR Green (Roche, Mannheim, Germany). β-Actin was used as an internal control for normalizing the fold change in the target gene mRNA levels. The mRNA levels of the target genes were analyzed using the $2^{-\Delta\Delta Ct}$ method. Supporting information displays the primer sequences used in the qRT-PCR. Primer sequences are shown in Table S2.

2.10 Histopathology and immunohistochemistry (IHC)

Tumor tissues and vital organs including the heart, liver, spleen, lung, and kidney were fixed in 4% paraformaldehyde at 4 °C. The specimens were then sectioned into 5 μm slices and embedded in paraffin for hematoxylin and eosin (H&E) staining and IHC. H&E staining was performed using H&E (obtained from Servicebio, Wuhan, China), with each stain applied for 6–8 min, followed by section dehydration and sealing. For IHC analysis, endogenous peroxidase activity was blocked as part of the antigen retrieval process. Subsequently, serum blocking, incubation with primary and secondary antibodies, and visualization were carried out. All images were acquired using a microscope from Nikon (Tokyo, Japan).

2.11 Western blotting analysis

Tumor tissue and B16F10 cells were lysed using a RIPA lysis buffer (RIPA:PMSF:protease inhibitor = 100:1:1, *V*/*V*) to extract total proteins. The protein concentration was determined using a BCA assay kit from Solarbio (Beijing, China), by measuring the absorbance at 562 nm using a microplate reader. The samples were separated by SDS-PAGE and transferred onto a PVDF membrane (Merck Microporous, Massachusetts, USA). The membrane was then blocked with 5% skim milk for approximately 1.5 h. Subsequently, it was incubated with primary antibodies at 4 °C for at least 12 h. Finally, the membrane was sequentially treated with horseradish peroxidase-conjugated secondary antibodies. After incubation with skim milk, primary antibodies, and secondary antibodies, the membrane was washed with TBST. Images were captured using an imaging system (Tanon5200, Shanghai, China), and the data were analyzed using ImageJ.

2.12 Molecular docking analysis

The CK and STING binding details were studied using AutoDock 4.2.6 technique. The 3D structure of CK was drawn in KingDraw 3.0, and the energy of the small molecule was minimized using the MM2 molecular mechanics method. The appropriate structure of STING for docking was selected from the Protein Data Bank (PDB ID: 4LOJ). Generate the map file in AutoDock Tools 1.5.6 software and set the centre and position of the grid box to find the appropriate active pocket. Run AutoDock 4.2.6 molecular docking software to perform molecular pairing according to the Lamarck genetic algorithm.

2.13 TUNEL assay

TUNEL staining of paraffin sections of mouse tumor tissue was performed using the apoptosis detection kit (Roche, Basel, Switzerland). In brief, sections were dewaxed, proteins were repaired, and membranes were broken. Then, a reaction solution containing terminal deoxynucleotidyl transferase enzyme, dUTP, and buffer (1:5:50, *V*/*V*) was added and incubated at a constant temperature of 37 °C for 2 h. The nuclei were then re-stained with diamidino phenylindole (DAPI) and finally sealed with an anti-fluorescence quencher (Service Bio, Wuhan, China). Staining was observed, and images were acquired using a fluorescence microscope (Nikon).

2.14 Statistical analysis

All data are given as mean ± standard deviation (SD). Differences between groups were compared using One-way ANOVA. Significant differences were analyzed using SPSS 19.0, and $P < 0.05$ were considered statistically significant. Graphs were plotted using GraphPad Prism 8.0.

3. Results

3.1 CK inhibits the proliferation of B16F10 in vitro

To investigate the potential inhibitory effect of CK on the *in vitro* growth of melanoma cells, a cytotoxic assay (MTT assay) was conducted using B16F10 cells treated with varying concentrations of CK for 24 or 48 h. The findings demonstrated a time- and dose-dependent inhibition of B16F10 cell proliferation by CK (Fig. 1B). Additionally, AO/EB staining revealed a gradual decrease in the number of cells exhibiting green fluorescence, accompanied by a corresponding increase in the number of cells displaying red fluorescence, as CK concentration increased (Fig. 1C). Similarly, Hoechst 33324 staining demonstrated enhanced blue fluorescent intensity, nuclear cohesion (green arrow) and nuclear fragmentation (red arrow) in cells treated with CK, indicative of cell death (Fig. 1D). In the wound-healing assay, B16F10 cells were treated with CK at concentrations of 30 and 60 μmol/L. The results exhibited a significant delay in wound closure at 12 and 24 h compared to untreated cells, further supporting the potential therapeutic application of CK in inhibiting melanoma cell proliferation.

3.2 Anti-tumor activity of CK in vivo

To investigate the potential inhibitory effect of CK on melanoma proliferation *in vivo*, tumor models were established in mice by injecting B16F10 cells (Fig. 2). As depicted in Fig. 2A, CK (40 and 80 mg/(kg·day)) and cyclophosphamide effectively suppressed the growth of subcutaneous tumors in mice compared to the Control group. Analysis of tumor weight and volume further confirmed significant reductions in the CK (40 and 80 mg/(kg·day)) and Cyclophosphamide groups compared to the Control group (Figs. 2B and C). The tumor weight inhibition rates were 66.73% (Cyclophosphamide group), 51.69% (L-CK group), and 71.72% (H-CK group), with no significant difference between the H-CK group and the Cyclophosphamide group. This suggests that a high dose of CK can achieve a melanoma inhibitory effect similar to cyclophosphamide. The body weight of tumor-bearing mice is presented in Fig. 2D, indicating that CK had no impact on the body weight compared to Normal group. IHC staining demonstrated a significant reduction in Ki-67 expression in the CK (40 and 80 mg/(kg·day)) and Cyclophosphamide groups, indicating inhibition of cell proliferation (Fig. 2E). Furthermore, histopathological examination of tumor tissues revealed tightly arranged cells in the CK (40 and 80 mg/(kg·day)) and Cyclophosphamide groups, while cells in the Control groups exhibited loose arrangement with gaps (Fig. 2E). No abnormalities were observed in the liver and kidney, which are major organs, of the H&E-stained Control group mice. However, cardiomyocytes appeared loosely arranged, the boundaries of the red and white medulla of splenic tissues were unclear, and alveolar structures displayed large areas of vacuoles. In contrast, the CK (40 and 80 mg/(kg·day)) groups exhibited neatly arranged cardiomyocytes and distinct bundles of hepatocytes. The boundaries of splenic tissues were clearly defined, alveoli were uniformly distributed, and glomeruli appeared normal. These observations suggest that CK did not induce significant toxicity in various organs. Thus, these findings demonstrate that CK effectively inhibits tumor development in mice with subcutaneous B16F10 tumors.

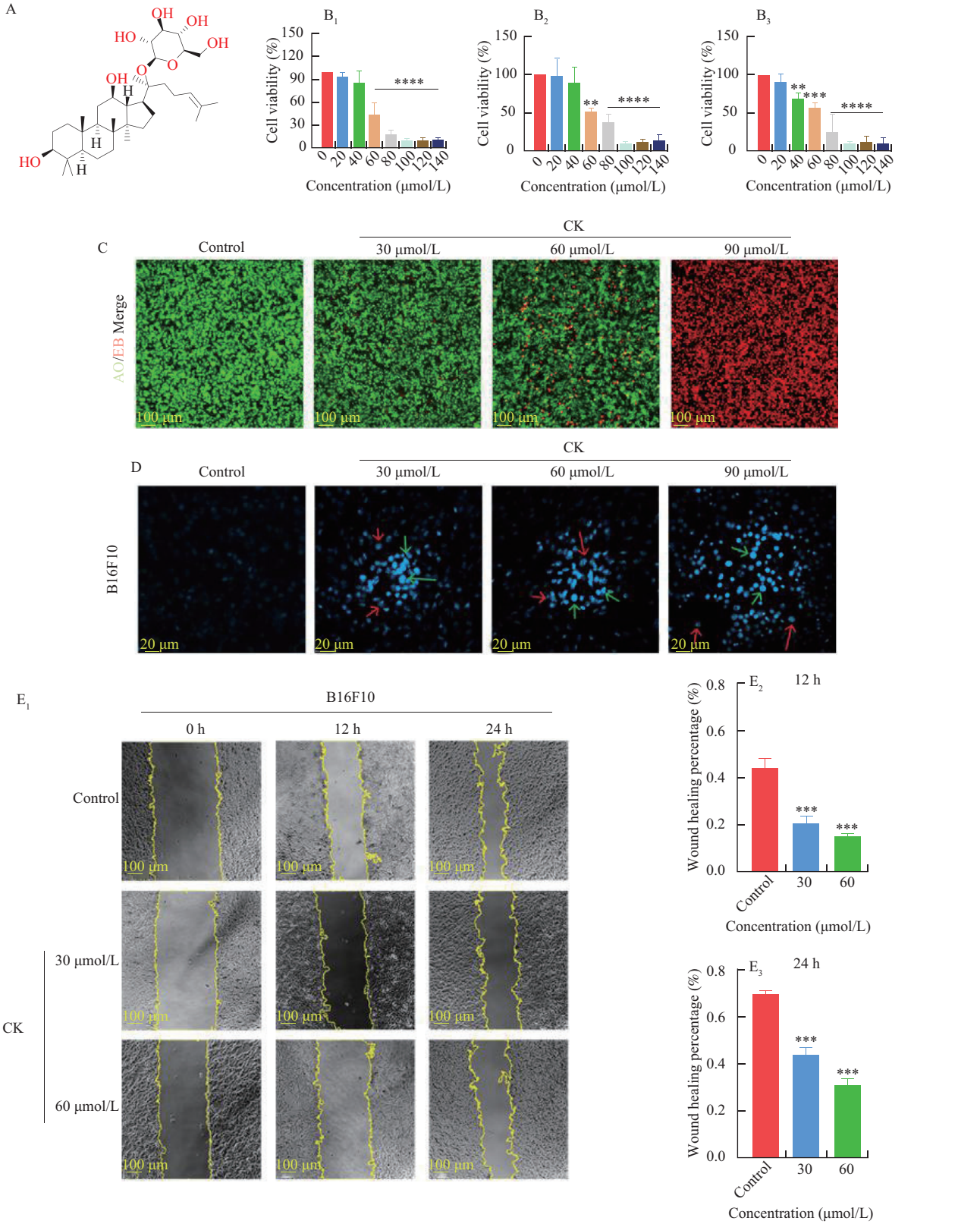

Fig. 1 CK significantly inhibits the proliferation of B16F10 *in vitro*. (A) Chemical structure of CK. (B_1-B_3) MMT assay for cell *via* bility. Different concentrations of CK (0, 20, 40, 60, 80, 100, 120, 140 μmol/L) were applied to B16F10 cells for 24, 48 and 72 h. (C) AO/EB staining was performed to observe the morphological changes of apoptotic cells after 24 h of CK action. Scale bar = 100 μm, 100×. (D) Morphological changes of apoptosis were analyzed by Hoechst 33324 staining after 0, 30, 60, 90 μmol/L CK action for 24 h. Scale bar = 20 μm, 400×. Red arrows represent nucleus fragmentation and green arrows represent nucleus coalescence. (E) Migration images of cells with or without CK at 0, 12, and 24 h. The yellow line is the edge of migration. Scale bar = 100 μm, 100×. All data are presented as means ± SD from at least 3 independent experiments. $^{**}P < 0.01$, $^{***}P < 0.001$, $^{****}P < 0.000\ 1$ compared with the control.

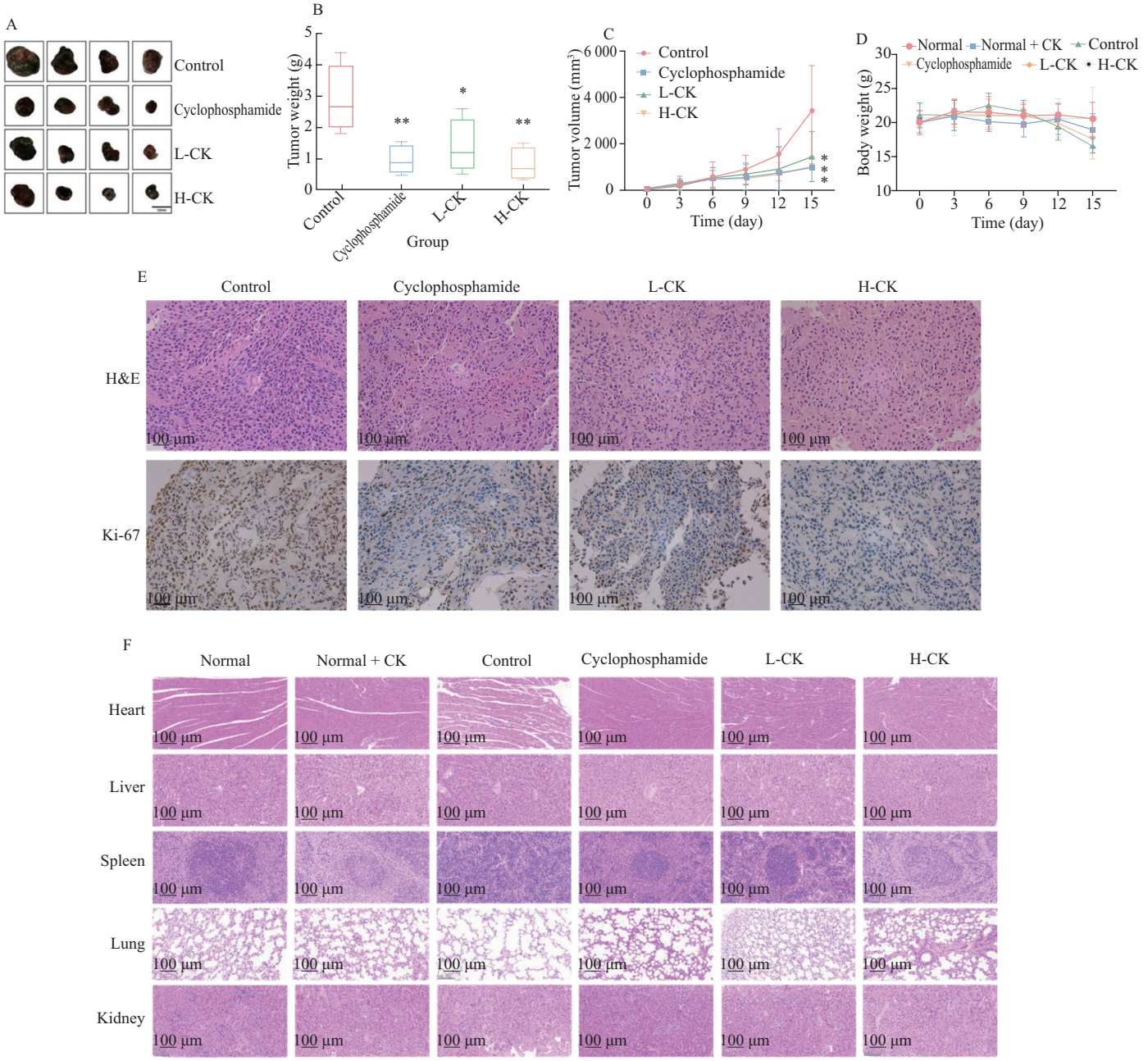

Fig. 2 *In vivo* growth inhibitory effect of CK. (A) Representative images of B16F10 graft tumors on 15 consecutive days ($n = 6$ mice/group). (B) Tumor weight. (C) Tumor volume. (D) Body weight. (E) Tumor tissues were stained for H&E and Ki-67 IHC. Scale bar = 100 μm. 200×. (F) H&E staining of major organs (heart, liver, spleen, lungs, kidneys) in each experimental group. Scale bar = 100 μm, 200×. All data are presented as means ± SD from at least 3 independent experiments. *$P < 0.05$, **$P < 0.01$, compared with the Control group.

3.3 CK induces cellular apoptosis in B16F10

To elucidate the mechanism underlying the inhibition of melanoma by CK, flow cytometry, TUNEL staining, and Western blotting were employed. Excessive levels of ROS can induce apoptosis in cancer cells[23–24]. To demonstrate the induction of ROS production by CK, intracellular ROS levels were assessed using DCFH-DA staining and flow cytometry. As depicted in Fig. 3A, the fluorescence intensity of DCFH-DA in B16F10 cells treated with CK (30 and 60 μmol/L) was enhanced compared to the control group, indicating elevated ROS levels. Consistent with the fluorescence staining results, flow cytometry analysis demonstrated that CK increased ROS accumulation in a concentration-dependent manner (Fig. 3B). Moreover, CK treatment significantly reduced the proportion of cells with decreased mitochondrial membrane potential compared to the control group (Fig. 3C). Elevated ROS levels and decreased mitochondrial membrane potential are characteristic features of

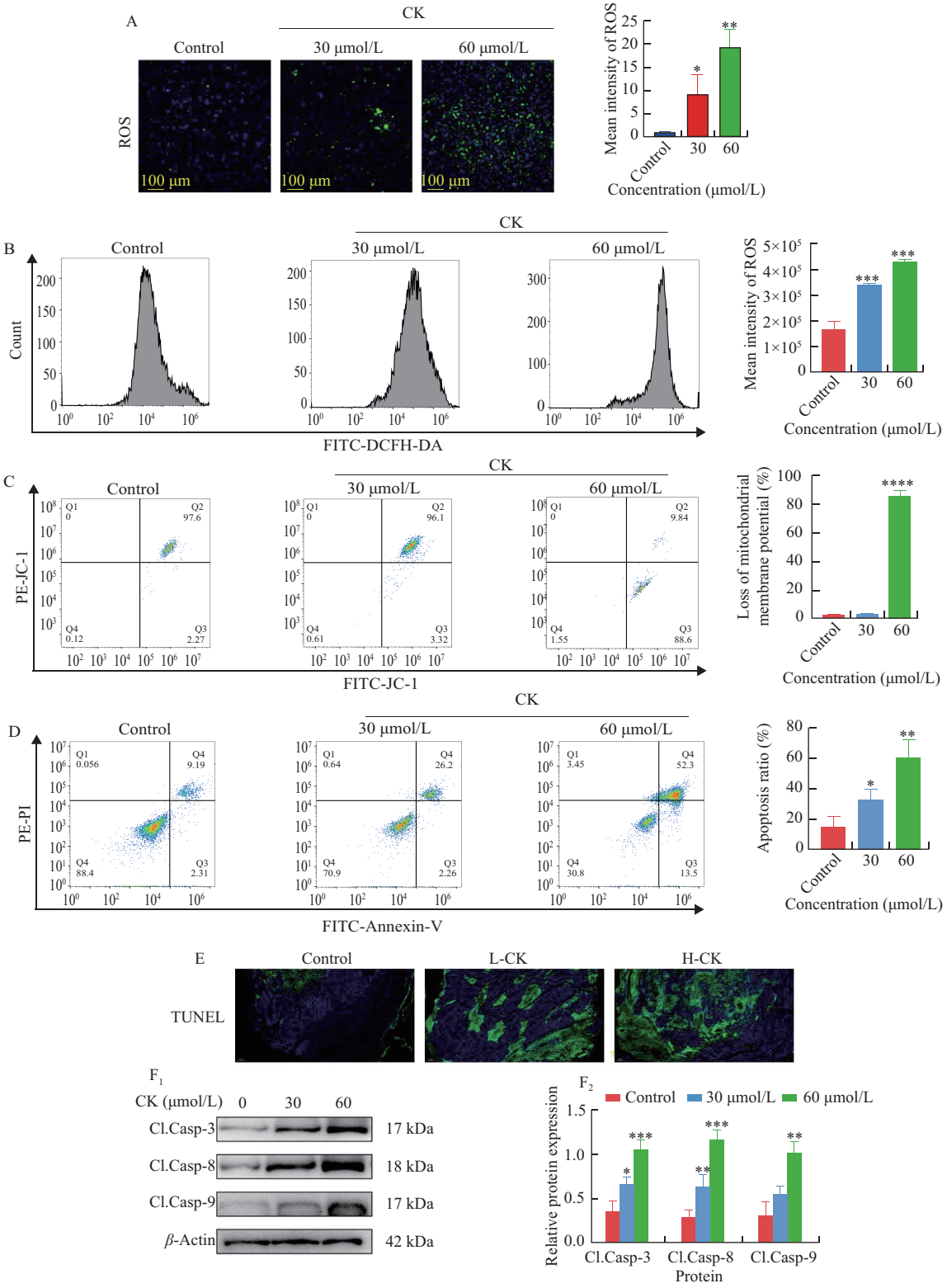

Fig. 3 CK induces apoptosis in melanoma cells. (A) Detected by DCFH-DA fluorescent probe ROS production. Changes in ROS levels in B16F10 cells after 24 h of 30 and 60 μmol/L CK action were observed by fluorescence microscopy. Scale bar = 100 μm, 100× magnification. (B) Cellular ROS production after the action of different concentrations of CK was analyzed by flow cytometry. (C) Detection of mitochondrial membrane potential with JC-1 fluorescent probe. Changes in mitochondrial membrane potential of B16F10 cells 24 h after the action of different concentrations of CK were analyzed by flow cytometry. (D) B16F10 cells were treated with CK for 24 h and analyzed by flow cytometry awakening. The histogram shows the proportion of apoptotic cells. (E) Apoptosis of tumor cells was analyzed by TUNEL. Scale bar = 200 μm, 50×. (F-G) Western blotting was used to detect the expression of apoptosis-related proteins *in vitro* and *in vivo*. (F_1) Western blotting to analyze the expression levels of Cl.Casp-3, Cl.Casp-8, and Cl.Casp-9 (*β*-actin was used as an endogenous reference); (F_2) statistical analysis of relative protein expression levels. (G_1) Western blotting to analyze the expression levels of Cl.Casp-3, Cl.Casp-8, and Cl.Casp-9 (*β*-actin was used as an endogenous reference); (G_2) statistical analysis of relative protein expression levels. All data are presented as means ± SD from at least three independent experiments. *$P < 0.05$, **$P < 0.01$, ***$P < 0.001$, ****$P < 0.000\ 1$ compared with the Control.

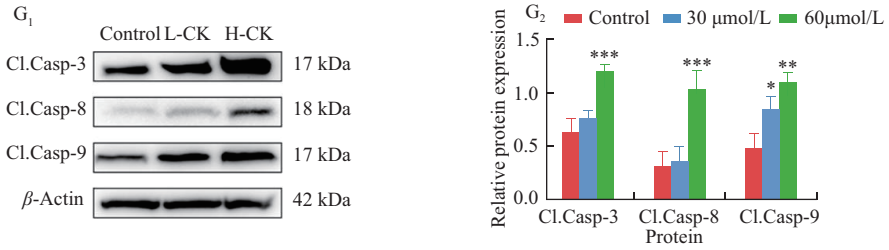

Fig. 3 (*Continued*)

apoptosis[25]. Flow cytometry results further indicated that CK can induce apoptosis in B16F10 cells (Fig. 3D). TUNEL staining revealed a gradual increase in green fluorescence in the CK (40 and 80 mg/(kg·day)) groups compared to the Control group, indicating enhanced levels of apoptosis *in vivo* (Fig. 3E). Western blotting was performed to assess apoptosis-related proteins and demonstrated that CK significantly increased the expression of cleaved-Caspase-9, cleaved-Caspase-8, and cleaved-Caspase-3 both *in vitro* (Fig. 3F) and *in vivo* (Fig. 3G). In conclusion, the aforementioned findings suggest that CK effectively inhibits tumor growth by promoting apoptosis in both *in vitro* and *in vivo* settings.

3.4 CK activation of cGAS-STING signaling

Ginsenosides have been found to enhance the body's immune response and induce apoptosis in tumor cells. To assess the impact of CK on the immune function of melanoma, the transcriptional levels of type I interferon (IFN-β) and chemokines (CCL-5, CXCL-10) were examined using real-time PCR assay. As depicted in Fig. 4A, the expression levels of *IFN-β*, *CCL-5*, and *CXCL-10* in B16F10 melanoma cells increased with the escalating concentration of CK administered for 24 h. Interestingly, similar results were observed *in vivo*, where the expression levels of *IFN-β*, *CCL-5*, and *CXCL-10* in mouse tumor tissues increased with the increasing concentration of CK administered (Fig. 4B). Activation of the cGAS-STING signaling pathway plays a crucial role in antitumor immunity[26]. Activation of cGAS by tumor DNA leads to the production of type I interferons and chemokines, which in turn stimulate tumor-specific T cell proliferation and recruitment to the tumors[27]. To investigate whether CK regulates IFN-β and chemokines by modulating the cGAS-STING signaling pathway, the gene expression levels of key markers of this pathway were examined. Real-time PCR results demonstrated that, compared to the control group, the genes *cGAS*, *STING*, and *TBK1* were abundantly expressed in B16F10 melanoma cells after CK administration (Fig. 4C). Similarly, the transcriptional expression of *cGAS*, *STING*, and *TBK1* was significantly increased in tumor tissues in a dose-dependent manner following CK administration (Fig. 4D).

The inhibition of the cGAS-STING pathway has been observed in the majority of tumors, potentially facilitating tumor progression[28]. Upon activation, STING recruits TBK1, which phosphorylates both STING and the transcription factor IFN regulatory factor 3 (IRF3). Phosphorylated IRF3 forms dimers and translocates into the nucleus, initiating the expression of type Ⅰ IFNs and inflammatory cytokines, thereby triggering antiviral immune responses[29]. To investigate the impact of CK on cGAS-STING pathway protein levels, Western blotting experiments were conducted to assess the expression levels of key proteins. Analysis of tumor tissues *via* Western blotting revealed a significant increase in the levels of p-STING, p-TBK1, and p-IRF3 in the tumor tissues treated with CK (40 and 80 mg/(kg·day)) compared to the Control group (Fig. 4E). To further explore the regulatory role of STING in this pathway, the protein levels of p-STING, p-TBK1, and p-IRF3 were measured in cells treated with the STING inhibitor C 170. The data demonstrated that the addition of C 170 inhibited the expression of p-STING, p-TBK1, and p-IRF3. However, the combined addition of CK (60 μmol/L) and the STING inhibitor resulted in a significant increase in the expression of p-STING, p-TBK1, and p-IRF3 (Fig. 4F). These findings suggert that CK has the ability to activate the cGAS-STING pathway. To investigate the binding details between CK and STING, AutoDock 4.2.6 was employed. The predicted binding affinity between CK and STING was determined to be –6.59 kcal/mol, indicating a strong affinity between the two. Fig. 4G illustrates the

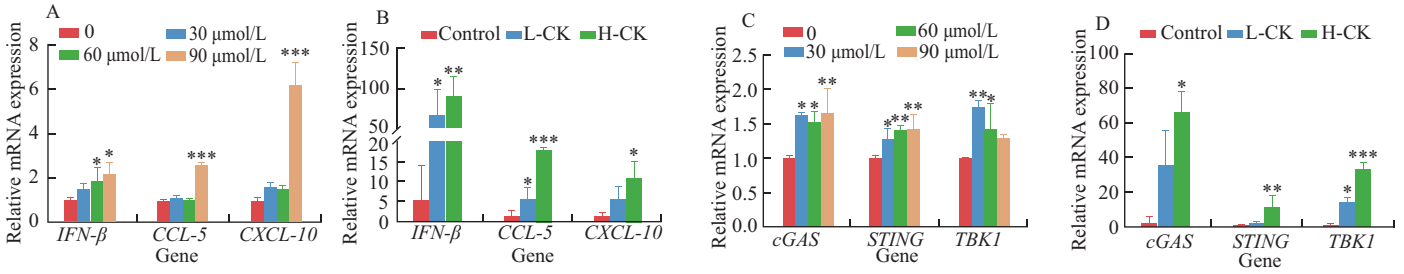

Fig. 4 CK promotes STING expression. (A-B) Effects of CK on *IFN-β*, *CCL-5* and *CXCL-10* gene expression levels *in vitro* and *in vivo*. (C-D) Effect of CK on the expression levels of *cGAS*, *STING* and *TBK1* genes *in vitro* and *in vivo*. (E_1) Western blotting to analyze the expression levels of key STING-TBK1-IRF3 proteinsn (*β*-actin was used as an endogenous reference); (E_2-E_3) statistical analysis of relative protein expression levels. (F_1) B16F10 cells were incubated with CK with and without C 170 (1 μmol/L), respectively (60 μmol/L) treatment, and the levels of STING, p-STING, TBK1, p-TBK1, IRF3, and p-IRF3 were detected by Western blotting (*β*-actin was used as an endogenous reference); (F_2-F_3) statistical analysis of relative protein expression levels. (G) CK-STING in 3D docking mode. (H) CK-STING in 2D docking mode. All data are presented as means ± SD from at least 3 independent experiments. *$P < 0.05$, **$P < 0.01$, ***$P < 0.001$ compared with the control. $^{\#\#}P < 0.01$, $^{\#\#\#}P < 0.001$ compared with the C 170.

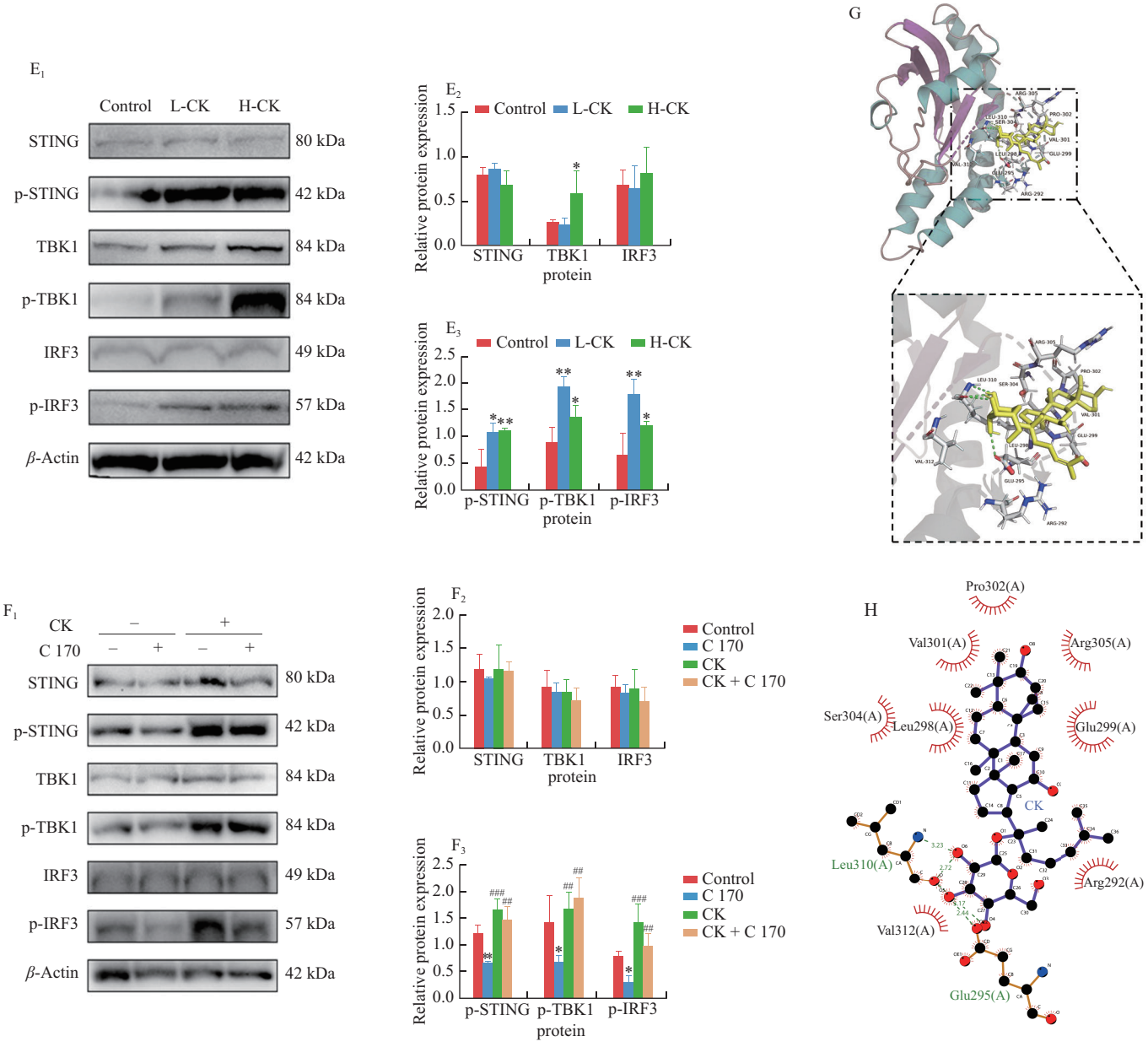

Fig. 4 (*Continued*)

hydrophobic surface of the CK-STING complex in 3D docking mode. The results indicate that CK interacts with amino acid residues surrounding the binding region. Hydrogen bonding plays a significant role in the structure and conformation of a substance, often leading to conformational changes in the molecule. As depicted in Fig. 4H, 2 hydrogen bonds were observed between CK and STING, facilitating the spontaneous formation of a stable structure. Based on these results, it can be inferred that STING plays a crucial role in the CK-mediated promotion of the cGAS-STING pathway.

3.5 CK promoted tumor lymphocyte infiltration

To evaluate the impact of CK on the tumor immune microenvironment, we examined the proportions of T lymphocytes. Flow cytometry was employed to identify different subsets of T lymphocytes within the tumor tissue. The CK (40 and 80 mg/(kg·day)) group exhibited increased proportions of $CD45^+$ lymphocytes, $CD3^+$ T cells, $CD45^+CD3^+CD4^+$ (T helper cells), and $CD45^+CD3^+CD8^+$ (cytotoxic T lymphocytes) (Fig. 5A). IHC staining further revealed that CK promotes the infiltration of $CD4^+$ and $CD8^+$ T cells into the tumor (Fig. 5B). Therefore, these findings suggest that CK modulates the proportions of T lymphocytes and mitigates immunosuppression. Taken together, the results indicate that CK may exert anti melanoma activity by promoting apoptosis and activating cGAS-STING pathway, and the possible mechanism is shown in Fig. 6.

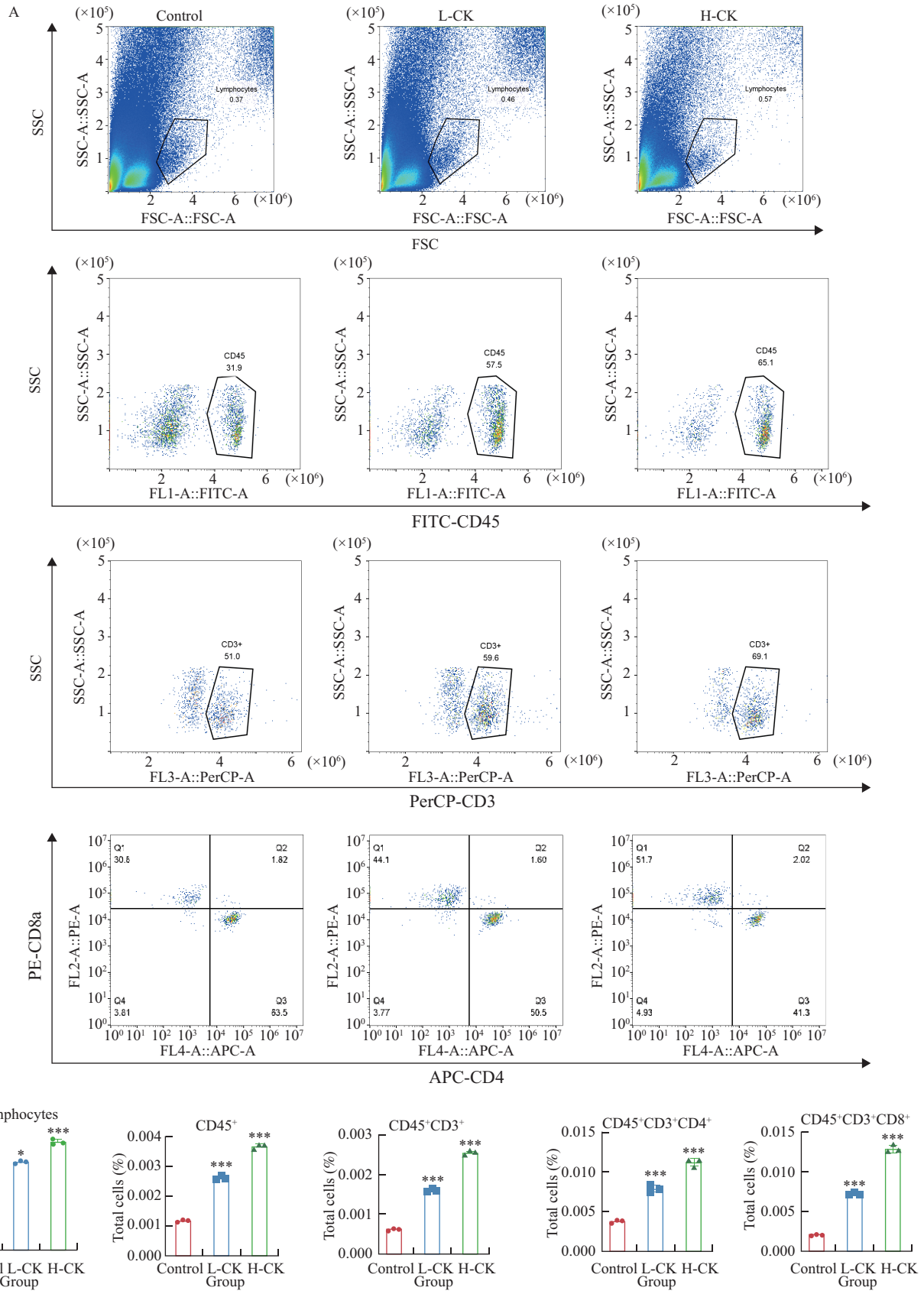

Fig. 5 CK promotes infiltration of tumor lymphocytes. (A) C57BL/6 mice were executed after 15 days, tumors were isolated, and lymphocyte infiltration was analyzed by flow cytometry with the indicated antibodies. The gating strategy and representative graphs are given in the text. Proportion of $CD45^+$, $CD45^+CD3^+$, $CD45^+CD3^+CD4^+$, $CD45^+CD3^+CD8^+$ cells in tumor tissues of each group ($n = 3$). (B) IHC staining of tumor tissues for CD4 and CD8 proteins. The quantitative analysis results of IHC are shown in the figure, with the *y*-axis representing relative integrated optical density (IOD). Scale bar = 100 μm, 100×. All data are presented as means ± SD from at least 3 independent experiments. $^*P < 0.05$, $^{**}P < 0.01$, $^{***}P < 0.001$ compared with the control.

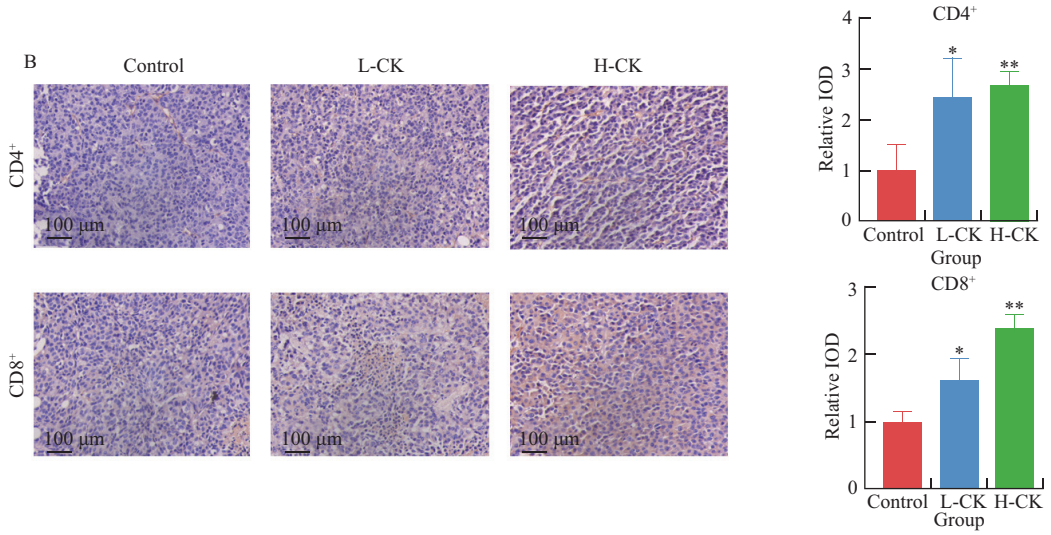

Fig. 5 (*Continued*)

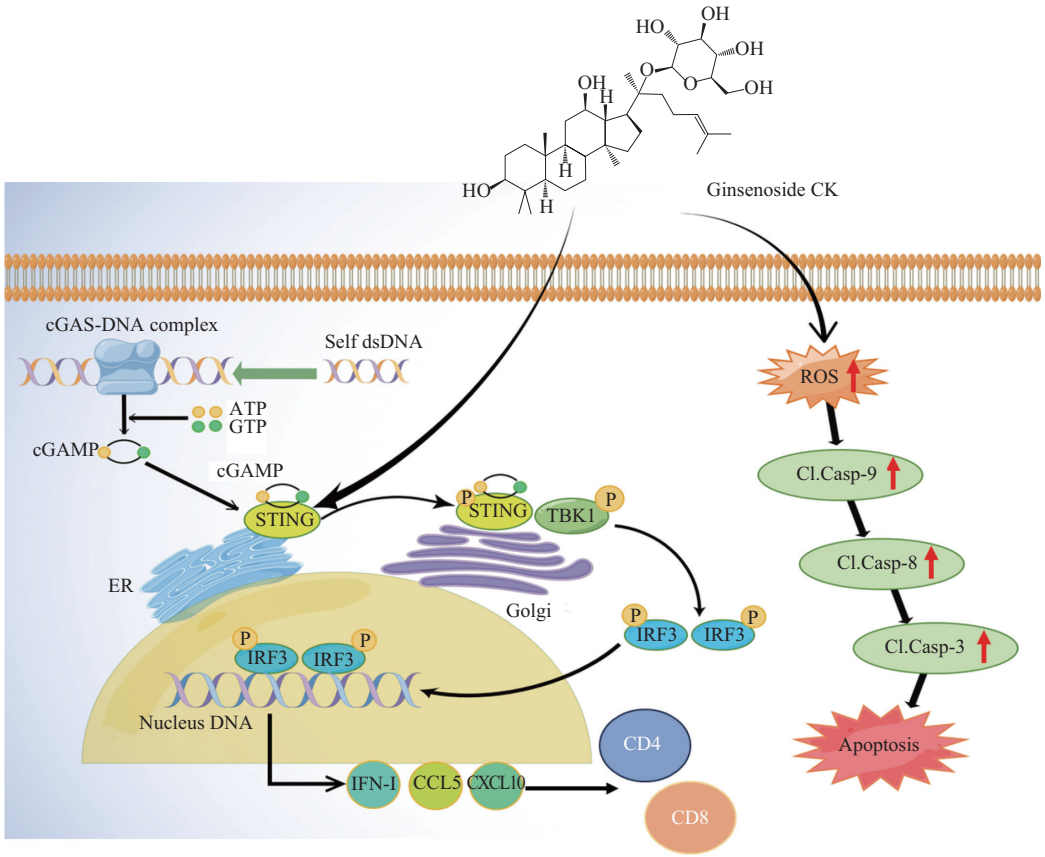

Fig. 6 Scheme of the proposed mechanism of action of ginsenoside CK in tumor immune microenvironment by Figdraw.

4. Discussion

In numerous studies, herbal formulations, medicinal plants, and their bioactive constituents have exhibited remarkable efficacy in cancer treatment[14,30–31]. These interventions have been shown to enhance quality of life and extend survival for cancer patients while having minimal adverse effects[31–32]. Ginsenosides are active compounds derived from the ginseng plant, and among them, CK stands out as a rare ginsenoside with notable anti-cancer properties[33-34]. However, the precise mechanisms by which CK attenuates tumor growth by modulating the immune microenvironment remain poorly understood. In this investigation, it was observed that CK not only directly induced apoptosis in B16F10 cells through the Caspase pathway, but also released cytokines by activating the cGAS-STING pathway of the tumor cells and enhanced the T-cell content in the tumor immune microenvironment. Moreover, our findings demonstrated that CK exhibited remarkable tumor suppression capabilities with low toxicity in mice. Collectively, these *in vitro* and *in vivo* findings suggest that CK holds promising potential as an anti-melanoma agent.

Among the various apoptotic signaling pathways, the mitochondrial apoptosis signaling pathway plays an indispensable role in inducing apoptosis in cancer cells[35]. Mitochondrial dysfunction leads to excessive production of ROS, resulting in oxidative stress and further exacerbating mitochondrial dysfunction, ultimately leading to apoptosis[36]. Cysteinyl asparaginase holds a distinctive position in both the mitochondrial endogenous apoptosis signaling pathway and the death receptor apoptosis signaling pathway, and its activation serves as a hallmark of apoptosis. ROS cause damage to the mitochondrial membrane, leading to a reduction in its integrity and a decline in mitochondrial membrane potential. Consequently, cytochrome C is released from the mitochondria into the cytoplasm, where it forms a complex with the Caspase-9 precursor, triggering the cleavage of Caspase-8 and Caspase-3, ultimately resulting in cell death[37]. Flow cytometry analysis revealed that CK promoted intracellular ROS elevation, decreased mitochondrial membrane potential, and increased the proportion of apoptotic cells (Figs. 3B-D). Western blotting analysis demonstrated that CK enhanced the expression of Caspase-9, Caspase-8, and Caspase-3 proteins (Figs. 3F and G). These results indicate that CK promotes apoptosis in a Caspase-dependent manner, both in *in vitro* and *in vivo* settings.

As previously documented, the regulation of the cGAS-STING signaling pathway is intricately linked to tumor immunity and represents a highly promising therapeutic target, as extensively reported in the literature[38]. Activation of the cGAS-STING pathway induces the secretion of IFN-β and chemokines by neoplastic cells[39]. Moreover, our initial investigation into B16F10 cells revealed an elevation in *STING* and *IFN-β* transcript levels upon treatment with CK. This observation suggests that CK may modulate the expression of *IFN-β* through the cGAS-STING signaling pathway. Subsequent Western blotting analysis demonstrated that CK impacts the expression of p-STING, p-TBK1, and p-IRF3. Mechanistically, CK may initiate the phosphorylation of STING, leading to the translocation of p-STING from the endoplasmic reticulum to the Golgi apparatus. p-STING then phosphorylates TBK1, which in turn promotes the phosphorylation of IRF3. Consequently, p-IRF3 translocates to the nucleus, inducing the expression of IFN-β and chemokines, thereby fostering anti-tumor immune responses[40]. Notably, STING plays a pivotal role in this cascade, regulating the expression of IFN-β and chemokines by modulating TBK1 and IRF3 phosphorylation, thereby orchestrating the body's anti-tumor immune response[41]. By employing STING inhibitors, we observed that CK enhances the expression of TBK1 and IRF3 phosphorylation by modulating STING phosphorylation. Furthermore, we investigated the binding affinity between CK and STING through molecular docking analysis. The obtained binding energy was calculated to be –6.59 kcal/mol, indicating the occurrence of spontaneous binding between these entities. The presence of hydrogen bonding further substantiates the formation of a stable structure. Collectively, these investigations suggest that the cGAS-STING signaling pathway holds promise as a potential clinical target for melanoma treatment. Notably, the expression of IFN-β and chemokines is closely associated with immune infiltration within the tumor microenvironment. Consequently, we assessed the infiltration of $CD4^+$ T cells and $CD8^+$ T cells in tumors, and our data indicate that CK therapy enhances the ratio of $CD4^+$ T lymphocytes to $CD8^+$ T lymphocytes within the tumor milieu.

In summary, CK exhibited potent inhibitory effects on melanoma cell proliferation, facilitated melanoma cell apoptosis, and significantly reduced tumor burden in murine models. Notably, we have elucidated the *in vitro* and *in vivo* mechanisms underlying the immunomodulatory properties of CK. Specifically, CK induced apoptosis by stimulating intracellular ROS generation in melanoma cells and concurrently attenuating mitochondrial membrane potential, thereby triggering the mitochondrial apoptotic pathway. Simultaneously, CK activated downstream phosphorylation events of TBK1 and IRF3 by upregulating STING expression and facilitating STING phosphorylation, consequently promoting the production of IFN-β and chemokines. This orchestrated immune response facilitated the recruitment of immune cells towards tumor cells, ultimately leading to their eradication. In conclusion, CK not only promotes melanoma cell apoptosis but also enhances the presence of immune cells within the tumor microenvironment, thereby playing a pivotal role in anti-melanoma activities. Consequently, CK holds great potential as an effective natural product for melanoma treatment, offering promising prospects for the management of melanoma patients.

Conflict of interest

The authors declare that they have no known competing financial interests that could influence this work.

Acknowledgements

This work was supported by the National Natural Science Foundation of China (22278335 and 22378329) and Scientific Research Program Funded by Education Department of Shaanxi Provincial Government (23JK0691).

Appendix A. Supplementary data

Supplementary data associated with this article can be found, in the online version, at http://doi.org/10.26599/FSHW.2025.9250480.

References

[1] H. Sung, J. Ferlay, R.L. Siegel, et al., Global cancer statistics 2020: globocan estimates of incidence and mortality worldwide for 36 cancers in 185 countries, CA Cancer J. Clin. 71 (2021) 209-249. https://doi.org/10.3322/caac.21660.

[2] M.G. Davey, N. Miller, N.M. McInerney, A review of epidemiology and cancer biology of malignant melanoma, Cureus 13 (2021) e15087. https://doi.org/10.7759/cureus.15087.

[3] A. Bansal, M.C. Simon, Glutathione metabolism in cancer progression and treatment resistance, J. Cell Biol. 217 (2018) 2291-2298. https://doi.org/10.1083/jcb.201804161.

[4] T. Abe, A. Harashima, T. Xia, et al., Sting recognition of cytoplasmic DNA instigates cellular defense, Mol. Cell. 50 (2013) 5-15. https://doi.org/10.1016/j.molcel.2013.01.039.

[5] S. Yum, M. Li, A.E. Frankel, et al., Roles of the cgas-sting pathway in cancer immunosurveillance and immunotherapy, Annu. Rev. Cancer Biol. 3 (2019) 323-344. https://doi.org/10.1146/annurev-cancerbio-030518-055636.

[6] A. Ablasser, Z.J.J. Chen, Cgas in action: expanding roles in immunity and inflammation, Science 363 (2019) eaat8657. https://doi.org/10.1126/science.aat8657.

[7] E.C. Carroll, L. Jin, A. Mori, et al., The vaccine adjuvant chitosan promotes cellular immunity *via* DNA sensor cgas-sting-dependent induction of type I interferons, Immunity 44 (2016) 597-608. https://doi.org/10.1016/j.immuni.2016.02.004.

[8] D. Liu, H. Wu, C. Wang, et al., Sting directly activates autophagy to tune the innate immune response, Cell Death Differ. 26 (2019) 1735-1749. https://doi.org/10.1038/s41418-018-0251-z.

[9] B.J. Francica, A. Ghasemzadeh, A.L. Desbien, et al., TNFα and radioresistant stromal cells are essential for therapeutic efficacy of cyclic dinucleotide sting agonists in nonimmunogenic tumors, Cancer Immunol. Res. 6 (2018) 422-433. https://doi.org/10.1158/2326-6066.CIR-17-0263.

[10] C.H. Tang, J.A. Zundell, S. Ranatunga, et al., Agonist-mediated activation of sting induces apoptosis in malignant b cells, Cancer Res. 76 (2016) 2137-2152. https://doi.org/10.1158/0008-5472.CAN-15-1885.

[11] V. Kunzmann, H. Algül, E. Goekkurt, et al., Conversion rate in locally advanced pancreatic cancer (LAPC) after nab-paclitaxel/gemcitabine- or FOLFIRINOX-based induction chemotherapy (NEOLAP): final results of a multicenter randomised phase II AIO trial, Ann. Oncol. 30 (2019) v253. https://doi.org/10.1093/annonc/mdz247.

[12] T.L. Xia, H. Konno, G.N. Barber, Recurrent loss of sting signaling in melanoma correlates with susceptibility to viral oncolysis, Cancer Res. 76 (2016) 6747-6759. https://doi.org/10.1158/0008-5472.Can-16-1404.

[13] T.H. Lan, Z.W. Xu, Z. Wang, et al., Ginsenoside Rb1 prevents homocysteine-induced endothelial dysfunction *via* Pi3k/Akt activation and Pkc inhibition, Biochem. Pharmacol. 82 (2011) 148-155. https://doi.org/10.1016/j.bcp.2011.04.001.

[14] H. Jiang, P. Ma, Z. Duan, et al., Ginsenoside Rh4 suppresses metastasis of gastric cancer *via* SIX1-dependent TGF-β/Smad2/3 signaling pathway, Nutrients 14 (2022) 1564. https://doi.org/10.3390/nu14081564.

[15] X. Bai, R. Fu, Z. Duan, et al., Ginsenoside Rh4 alle *via* tes antibiotic-induced intestinal inflammation by regulating the TLR4-Myd88-MAPK pathway and gut microbiota composition, Food Funct. 12 (2021) 2874-2885. https://doi.org/10.1039/d1fo00242b.

[16] A. Zhu, Z. Duan, Y. Chen, et al., Ginsenoside Rh4 delays skeletal muscle aging through SIRT1 pathway, Phytomedicine 118 (2023) 154906. https://doi.org/10.1016/j.phymed.2023.154906.

[17] Y. Liu, J. Deng, D. Fan, Ginsenoside Rk3 ameliorates high-fat-diet/streptozocin induced type 2 diabetes mellitus in mice *via* the AMPK/Akt signaling pathway, Food Funct. 10 (2019) 2538-2551. https://doi.org/10.1039/c9fo00095j.

[18] K.S. Kang, J. Ham, Y.J. Kim, et al., Heat-processed panax ginseng and diabetic renal damage: active components and action mechanism, J. Ginseng Res. 37 (2013) 379-388. https://doi.org/10.5142/jgr.2013.37.379.

[19] M.Y. Kim, J.Y. Cho, 20*S*-Dihydroprotopanaxadiol, a ginsenoside derivative, boosts innate immune responses of monocytes and macrophages, J. Ginseng Res. 37 (2013) 293-299. https://doi.org/10.5142/jgr.2013.37.293.

[20] Y. Wan, D. Liu, J. Xia, et al., Ginsenoside CK, rather than Rb1, possesses potential chemopreventive activities in human gastric cancer *via* regulating PI3K/AKT/NF-κB signal pathway, Front. Pharmacol. 13 (2022) 1042351. https://doi.org/10.3389/fphar.2022.977539.

[21] B. Zhang, R.Z. Fu, Z.G. Duan, et al., Ginsenoside CK induces apoptosis in triple-negative breast cancer cells by targeting glutamine metabolism, Biochemical. Pharmacology 202 (2022) 115101. https://doi.org/10.1016/j.bcp.2022.115101.

[22] J.J. Zhang, X.X. Ma, D.D. Fan, Ginsenoside CK inhibits hypoxia-induced epithelial-mesenchymal transformation through the HIF-1α/NF-κB feedback pathway in hepatocellular carcinoma, Foods 10 (2021) 1195. https://doi.org/10.3390/foods10061195.

[23] D. Sunilkumar, G. Drishya, A. Chandrasekharan, et al., Oxyresveratrol drives caspase-independent apoptosis-like cell death in MDA-MB-231 breast cancer cells through the induction of ros, Biochem. Pharmacol. 173 (2020) 113724. https://doi.org/10.1016/j.bcp.2019.113724.

[24] Q. Wu, J. Deng, D. Fan, et al., Ginsenoside Rh4 induces apoptosis and autophagic cell death through activation of the ROS/JNK/p53 pathway in colorectal cancer cells, Biochem. Pharmacol. 148 (2018) 64-74. https://doi.org/10.1016/j.bcp.2017.12.004.

[25] Y. Che, Y. Tian, R. Chen, et al., IL-22 ameliorated cardiomyocyte apoptosis in cardiac ischemia/reperfusion injury by blocking mitochondrial membrane potential decrease, inhibiting ros and cytochrome c, Biochim. Biophys. Acta Mol. Basis Dis. 1867 (2021) 166171. https://doi.org/10.1016/j.bbadis.2021.166171.

[26] F. Shi, J. Su, J. Wang, et al., Activation of sting inhibits cervical cancer tumor growth through enhancing the anti-tumor immune response, Mol. Cell Biochem. 476 (2021) 1015-1024. https://doi.org/10.1007/s11010-020-03967-5.

[27] N. Gehrke, C. Mertens, T. Zillinger, et al., Oxidative damage of DNA confers resistance to cytosolic nuclease trex1 degradation and potentiates sting-dependent immune sensing, Immunity 39 (2013) 482-495. https://doi.org/10.1016/j.immuni.2013.08.004.

[28] T.L. Xia, H. Konno, J. Ahn, et al., Deregulation of sting signaling in colorectal carcinoma constrains DNA damage responses and correlates with tumorigenesis, Cell Reports 14 (2016) 282-297. https://doi.org/10.1016/j.celrep.2015.12.029.

[29] O. Demaria, A. De Gassart, S. Coso, et al., Sting activation of tumor endothelial cells initiates spontaneous and therapeutic antitumor immunity, PNAS 112 (2015) 15408-15413. https://doi.org/10.1073/pnas.1512832112.

[30] J. Chen, Z. Duan, Y. Liu, et al., Ginsenoside Rh4 suppresses metastasis of esophageal cancer and expression of c-Myc *via* targeting the Wnt/*β*-catenin signaling pathway, Nutrients 14 (2022) 3042. https://doi.org/10.3390/nu14153042.

[31] X. Xue, Y. Liu, L. Qu, et al., Ginsenoside Rh3 inhibits lung cancer metastasis by targeting extracellular signal-regulated kinase: a network pharmacology study, Pharmaceuticals 15 (2022). https://doi.org/10.3390/ph15060758.

[32] H. Lu, H. Yin, L. Qu, et al., Ginsenoside Rk1 regulates glutamine metabolism in hepatocellular carcinoma through inhibition of the ERK/c-Myc pathway, Food Funct. 13 (2022) 3793-3811. https://doi.org/10.1039/d1fo03728e.

[33] J.H. Huang, D.L. Pan, F. Liu, et al., Ginsenoside compound K inhibits the proliferation, migration and invasion of ECA109 cell *via* VEGF-A/PI3K/Akt pathway, J. Cardiothorac. Surg. 17 (2022) 99. https://doi.org/10.1186/s13019-022-01846-2.

[34] C. Li, Y.C. Dong, L.B. Wang, et al., Ginsenoside metabolite compound K induces apoptosis and autophagy in non-small cell lung cancer cells *via* AMPK-MTOR and JNK pathways, Biochem. Cell Biol. 97 (2019) 406-414. https://doi.org/10.1139/bcb-2018-0226.

[35] Y. Zhu, Y. Jiang, L. Shi, et al., 7-*O*-Geranylquercetin induces apoptosis in gastric cancer cells *via* ROS-MAPK mediated mitochondrial signaling pathway activation, Biomed Pharmacother. 87 (2017) 527-538. https://doi.org/10.1016/j.biopha.2016.12.095.

[36] Y. Zhao, X. Ye, Z. Xiong, et al., Cancer metabolism: the role of ROS in DNA damage and induction of apoptosis in cancer cells, Metabolites 13 (2023) 796. https://doi.org/10.3390/metabo13070796.

[37] B.C. Schimming, M.L.A. Cirino, F.S. Lizarte Neto, et al., Chronic alcoholism associated with diabetes induced apoptosis in the corpus cavernosum of rats, Acta Cir. Bras. 35 (2020) e202000805. https://doi.org/10.1590/s0102-865020200080000005.

[38] K.W. Ng, E.A. Marshall, J.C. Bell, et al., cGAS-STING and cancer: dichotomous roles in tumor immunity and development, Trends Immunol. 39 (2018) 44-54. https://doi.org/10.1016/j.it.2017.07.013.

[39] S.R. Woo, M.B. Fuertes, L. Corrales, et al., Sting-dependent cytosolic DNA sensing mediates innate immune recognition of immunogenic tumors, Immunity 41 (2014) 830-842. https://doi.org/10.1016/j.immuni.2014.10.017.

[40] E.N. Chin, A. Sulpizio, L.L. Lairson, Targeting sting to promote antitumor immunity, Trends Cell Biol. 33 (2023) 189-203. https://doi.org/10.1016/j.tcb.2022.06.010.

[41] L. Corrales, L.H. Glickman, S.M. McWhirter, et al., Direct activation of sting in the tumor microenvironment leads to potent and systemic tumor regression and immunity, Cell Rep. 11 (2015) 1018-1030. https://doi.org/10.1016/j.celrep.2015.04.031.